



Research Article

## Studying the influence of using metal foam baffles on the performance of double-pipe heat exchanger

Zuhair S. RABEEAH<sup>1,\*</sup> , Abbas J. JUBEAR<sup>1</sup> , Hussain R. AL-BUGHARBEE<sup>1</sup> 

<sup>1</sup>Department of Mechanical Engineering, Wasit University, Wasit, 52005, Iraq

### ARTICLE INFO

#### Article history

Received: 11 November 2023

Revised: 29 March 2024

Accepted: 30 March 2024

#### Keywords:

Copper Foam Baffles; Heat Transformer Rate Enhancement; Local Thermal Equilibrium; Numerical Investigation

### ABSTRACT

The enhancement of the thermal performance of heat exchangers has a great importance to the researchers. This is because improving the performance will lead to increasing the efficiency of the application where the heat exchangers are used. In this study, the thermal and hydraulic performance of a double heat exchanger with open-cell copper foam baffles inside was investigated numerically and experimentally with water as operating fluid. The numerical simulation was conducted using ANSYS FLUENT 2020 R2 to simulate the water flow and temperature distribution in the heat exchanger at different configurations. These configurations included the completely and partially filled with metal foam with different foam properties such as pore density, baffle angle, and baffle thickness. The experimental work included the designing and building of the test rig and obtaining the temperature recordings which were used for comparison purposes. Results were obtained for temperature contours, velocity streamlines, Nusselt numbers, effectiveness, pressure drops, and friction factors at variable baffles angles ( $\beta = 60^\circ, 120^\circ, 180^\circ$ ), variable baffles thickness ( $t = 10, 20, 30\text{mm}$ ), and variables pore density (PPI=10, 20, 30, 40, 50PPI). They showed that as the volume of metal foam increases, the heat transfer rate ( $Q_{ave}$ ) and the pressure drop ( $\Delta p$ ) increases. In addition, the performance of the heat exchanger with a partially filled core was better than that in the completely filled case. On the other hand, when the metal foam volume decreases, the pressure drop decreases. Furthermore, it was observed that the heat transfer rate increases with the increase in pore density. Experimental results showed an enhancement in heat transfer rate in a double-pipe heat exchanger by 32.4% at 40PPI and  $\beta=180^\circ$ . There was also an enhancement in the Nusselt number value ( $Nu_{ave}$ ) by 117% due to the use of copper foam baffles.

**Cite this article as:** Rabeeah ZS, Jubear AJ, Al-Bugharbee HR. Studying the influence of using metal foam baffles on the performance of double-pipe heat exchanger. J Ther Eng 2025;11(1):196–214.

\*Corresponding author.

\*E-mail address: [zuhairsa302@uowasit.edu.iq](mailto:zuhairsa302@uowasit.edu.iq)

This paper was recommended for publication in revised form by Editor-in-Chief Ahmet Selim Dalkılıç



## INTRODUCTION

Recently, many industrial applications require small size and good performance heat exchangers. There are several strategies for improving heat transfer, including using porous material, extended surfaces, and rough surfaces. Numerous experimental and computational investigations have focused on the use of extended surfaces like fins. For a specific pumping power and flow rate, these studies examine the optimal ways to form and arrange these kinds of structures to enhance heat transfer. The major objective of these strategies is to increase the flow's turbulence or increase the heat transfer surface.

A porous material is one of the most important methods for improving heat transfer, according to several researchers [1]. Open-cell metal foams are one of these kinds of porous metals. They are distinguished by their physical, mechanical, and thermal properties including high thermal conductivity, high mixing of fluid flow, big porosity, large surface area, lightweight, and good structure. Therefore it was used in more types of heat exchangers with metal foam [2], and the device has micro parts [3] and heat sink heat exchangers [4].

Bousri et al. [5], used a numerical simulation to analyze the heat transmission in a parallel-plate heat exchanger with two distinct configurations where each includes four metal foam blocks positioned alternately on the top and bottom of the channel walls. The authors made use of the Brinkman-Forchheimer-extended Darcy model. They claimed that the second configuration, in which the blocks are positioned precisely at a distance from the channel walls provided better improvement of the cooling of the heat sources by forced convection. In addition, the same value of the coefficient of friction is observed for both configurations regardless of the Darcy number. BANERJEE & Diplina, 2021 [6], studied the heat transmission in a pipe containing a porous media and constant external heat flux. A quasi-thermal equilibrium model in a two-dimensional domain for the investigation. The Nusselt number was calculated at various porosity, pore density, Reynold's number, and solid and fluid thermal conductivity. Three PPI values were considered (i.e. 10 PPI, 40 PPI, and 60 PPI). The results showed that a larger pore density porous medium causes a higher pressure drop and Nusselt number. This was attributed to a decrease in the foam's fiber diameter and the increase in interfacial heat transfer between the fluid and solid phases.

Five samples of aluminum foam as wrapped tube heat exchangers were investigated by Chumpia & Hooman, 2014 [7]. They used foam with porosity (0.901,0.937) and pore density (20PPI) with various thickness (5-20) mm. Four of these tubes were made from Aluminum and the fifth as made from steel. The results indicate that when foam layer thickness increases, the overall thermal resistance for thermal efficiency drops, and higher pressure drop. A test rig of 18 discs with a thickness of 18.2mm of open-cell aluminum foam (10 and 40PPI) and porosity of 88.5% brazed to the

inner surface of a cylindrical aluminum pipe was experimentally researched by Arbak et al. [8]. The results were compared with a previously published study with 20PPI. Foam with 40PPI produced the highest heat transfer, Foam with 20PPI produced the lowest heat transfer, and Foam with 10PPI lay in the middle. By Ali and Ghashim 2023 [9], using a metal foam insert in a circular horizontal pipe, the effects of turbulent forced convection heat transfer were experimentally studied. Under conditions of heat flux (31.8) KW/m<sup>2</sup> and (42.4) KW/m<sup>2</sup> outside the pipe and water flow rates (3, 6, and 9 lpm) with an input temperature of (32°C), the Nusselt number and friction factor were investigated. (60cm) in length, (25cm) in diameter, and (1mm) meters in thickness make up a circular copper pipe. The foam has a porosity between (0.89 and 0.93) and pores per inch (10-40 PPI). According to the findings, metal foam with a copper content of 40 PPI increases the average Nusselt number by up to 73%, whereas metal foam with a 10 PPI increases it by just 63.74%. The pressure drop The variations in pressure. above, there is very little difference in between pipes with and without metal foam at 10 PPI, but the difference increases at 40 PPI. A micro-channel is the subject of numerical research by Alibeigi and Farahani [10] that involves injecting fluid through its lower wall. The results explained that the heat transfer increases with the increased thickness of the porous medium layer.

Hamzah and Nima [11], investigated experimentally by inserting copper metal foam fins (40 PPI) in a double-pipe heat exchanger's inner copper pipe at a 30° angle with the flow direction and they showed the effect of the heat transfer and pressure drop. They claimed that metal foam caused a slight increase in pressure drop. Arasteh et al. [12], numerically examined the optimum distribution to the constant volume of metal foam placed partly in both pipes of the double-pipe heat exchanger with dimensionless parameters. The water was a fluid operation on both sides of the heat exchanger with constant properties. The results were that partially filled heat exchangers with the optimum distribution of metal foams have less pressure drop and enhance heat transfer rate economically more than fully filled heat exchangers. Maid et al. [13], used ANSYS FLUENT 14.1 to numerically analyses heat transfer in a double-pipe heat exchanger with and without a porous medium. Inner, outer, and both tubes are filled with alumina beads. The results showed that the best effectiveness was with a porous media in both tubes and there were more pressure drops and an increasing in Nusselt number as compared to the case without the metal pad. The thermal performance of a fully filled double-pipe heat exchanger with metal foam has (0.8–0.95) as a porosity and (5–30PPI) as a pore density, was explored numerically by Chen et al. [14]. The uniform and non-uniform foam structures in the internal and external pipes were taken into account and studied. The authors claimed an increase in the effectiveness and pressure drop with lower porosity and large pore density. The performance of a double-pipe heat exchanger

with copper metal foam (15PPI) and (0.95) porosity, partially/periodically filled between the two pipes was experimentally tested by Farhan et al. [15]. The results explained that the convection heat transfer coefficient improved when using the metal foam. Alhusseney et al. [16], quantitatively examined the improvement of heat transfer within a double-pipe heat exchanger. They used porous material as isotropic and homogeneous rigid metal foam with porosity  $\geq 0.89$ . They used active and passive techniques and discovered that effectiveness increased and pumping energy was saved in comparison to heat exchangers that were completely filled.

To solve the low thermal conductivity of phase change materials PCMs, Abandani and Ganji [17], investigated the effects of using three-layer of PCMs inside a triplex-heat exchanger and their combination effect with Al6061 metal foam (porosity of 0.95). The results showed an 88% improvement in performance when compared to the case without metal foam. Mohammadi et al. [18], investigated numerically to heat transfer rate and the pressure drop along a shell-tubes heat exchanger with six baffles of porous media. Three values for the baffle cut (25%, 35%, and 50%), the permeability was as (10-9m<sup>2</sup>, 10-12m<sup>2</sup>, and 10-15m<sup>2</sup>), and the porosity was as (0.2, 0.5, and 0.8). The results showed that a lower percentage baffle cut (25%) can improve the heat transfer while limiting the pressure drop.

In three different types of shell-tubes heat exchangers with helical and segmental as well as clamping baffles, inclusion inside tubes, two variations included the porosity porous media and its radius, Naqvi and Wang [19], estimated and evaluated using aluminum foam. The researchers claimed that porous medium with certain porosity and size can improve heat transfer rate while decreasing pressure drop and that the outer pipe must be partially filled rather than fully filled with porous media. Tamkhade et al. [20], the performance evaluate of a double-pipe heat exchanger with an inner tube made of stainless steel, and an outer tube made of galvanized iron was investigated using numerical and CFD analysis. With hot water (80°C) and (2 lpm) in the inner tube and cold water (30°C) and (10 lpm) in the outer tube as the working fluids, nickel metal foam with (10 - 50PPI) as pore density and 0.9 porosity is used. The results explained that the heat transfer coefficient of the stream through the annular flow passage and overall heat transfer coefficient increased together with the rise in pore density. Fiedler et al. [21], investigated the effectiveness of a novel alloy of metal foam ZA27 with heat exchanger. Through a casting technique, open cell metal foam is bonded with a pipe, the foam's macroscopic density (1.28-1.36g/cm<sup>3</sup>) and an interconnected porosity (72-74 vol.%). a temperature different about 42 kelvin. The results showed an increase in heat transfer reach to 71%. while, overall performance was constrained by the poor heat transfer between the inner mass stream and the copper pipe, because of the relatively low contact surface. Zhou et al. [22] investigated metal foam-wrapped cylinders in a shell and tube condenser

under sloshing conditions, including rolling, pitching, yawing, swaying, heaving, and surging. Open-cell copper foams with pore densities of (5, 10, 20, and 40PPI) were brazed to a copper tube, and the sloshing angle ranged from 0° to 12°. The sloshing frequency varied from 0 to 0.33 Hz. The heat exchanger with 10PPI copper foam had the highest condensation heat transfer performance, indicating a 34%–54% increase in amount compared to the heat exchanger without metal foam.

As to the best of the authors of the present study, the research presents a wide investigation on the use of partially filled annuli which most of the previous literature lacks, particularly the use of cut-out baffles. In addition, the experimental work includes a modification in the connection of baffles to the outer pipe. This modification helps in securing a firm contact between the copper foam baffles and the inner surface of the outer pipe. The analysis covers using of baffles with various configurations in a double-pipe heat exchanger on the thermal performance and hydraulic performance. Compared to other literature, more parameters including the shape, size, and properties of copper foam baffles were examined. The baffle angle changes as  $\beta = (0^\circ, 60^\circ, 120^\circ, 180^\circ)$ , thickness varies as (10, 20, 30mm), pore density varies as (10-50PPI), and water flow rate varies as  $\dot{V} = (2, 3, 4, 5, 6)$  lpm.

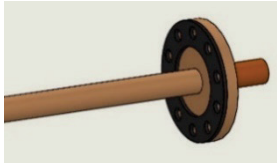
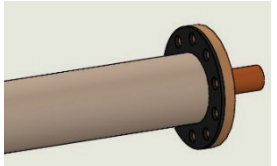
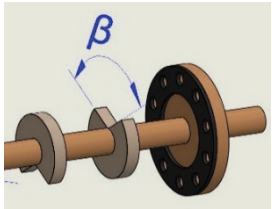
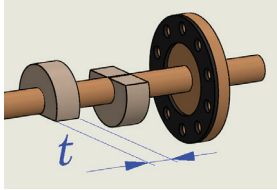
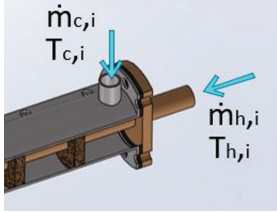
## NUMERICAL SIMULATION

To properly explain the technological challenge numerically, several partial differential equations must be solved, and numerical methods must be employed to solve these equations. The finite volume method is proved suitable for solving the continuity and momentum equations as well as energy equation through using the ANSYS 2020R2 software.

### Geometry

The dimensions of the geometry model of a double pipe heat exchanger (DPHX) provided by Ebieto et al. in 2020 [23] were employed and also used for the validation process. The geometry of the present study has two pipes; namely outer and inner. To provide a heat exchanger with full foam (HXWFF), the annular gap of the heat exchanger without foam (HXWOF) is firstly filled with open-cell copper foam that has (0.9) porosity and pore density was as (40PPI). Other cases of gap filling are also considered in the analysis where baffles are used. These baffles are nine pieces of copper foam baffles (CFB) with thicknesses (t) (10, 20, and 30mm) distributed uniformly across the annular region. These baffles are arranged using cut triangular pieces with various baffle angles ( $\beta$ ) (0°, 60°, 120°, and 180°) in opposition, and pore density was various as (10, 20, 30, 40, and 50PPI) to offer thirty examples until reach optimal heat exchanger (OPHX), as well as to examine various flow rates as ( $\dot{V} = 2-6$  lpm) in both pipes at the same time was done, the major cases are presented in Table 1.

**Table 1.** Figures and descriptions of the studied cases

Case	Description	3d View
1	Preliminary case Heat exchanger without foam (HXWOF) Flow rate $\dot{V} = (2, 3, 4, 5, 6)$ lpm	
2	Preliminary case Heat exchanger with full foam (HXWFF) Pore density = (40) PPI, Flow rate $\dot{V} = (2, 3, 4, 5, 6)$ lpm	
3	Case A Baffle angle $\beta = (0^\circ, 60^\circ, 120^\circ, 180^\circ)$ , Pore density = (10, 20, 30, 40, 50) PPI, Baffle thickness $t = 10$ mm, Flow rate $\dot{V} = 2$ lpm	
4	Case B Baffle angle $\beta = 180^\circ$ , Baffle thickness $t = (10, 20, 30)$ mm, Pore density = (10, 20, 30, 40, 50) PPI, Flow rate $\dot{V} = 2$ lpm	
5	Case C Baffle angle $\beta = 180^\circ$ , Baffle thickness $t = 10$ mm, Pore density = 40PPI, Flow rate $\dot{V} = (2, 3, 4, 5, 6)$ lpm	

**Mathematical Assumptions**

The descriptive analysis is based on the following assumptions:

- The conditions are steady state.
- The simulation in three-dimensional (x, y, z).
- Whether in the solid or fluid phases, thermophysical characteristics remain constant.
- Isotropic, rigid, homogeneous, and uniform metal foam.
- Fouling is disregarded.
- Viscosity dissipation and heat generation are ignored.
- The flow is turbulent.
- The employment of the local thermal non-equilibrium (LTNE) model in conjunction with energy equations.

**Governing Equations**

They are provided for analysis of fluid flow with heat transfer. The Navier-Stokes equation describes the water

flow field in the fluid area, whereas the volume-averaged generalized momentum equation that describes the flow field within isotropic homogeneous porous materials is defined by the Brinkman-Forchheimer extended Darcy model. These Governing Equations (1-7) are:

- Conservation of mass

Any closed system's mass is constant and does not fluctuate over time according to the laws of mass conservation [24]:

$$\frac{\partial v_x}{\partial x} + \frac{\partial v_y}{\partial y} + \frac{\partial v_z}{\partial z} = 0 \tag{1}$$

- Momentum equations

The change rate in momentums equals the net forces that act on a body according to Navier-Stokes equations and Newton's second law of motion [25]:

In X-direction



$$\frac{1}{\varepsilon^2} (V_x \frac{\partial V_x}{\partial x} + V_y \frac{\partial V_x}{\partial y} + V_z \frac{\partial V_x}{\partial z}) = -\frac{\partial p}{\partial x} + \frac{1}{\varepsilon Re} \left( \frac{\partial^2 V_x}{\partial x^2} + \frac{\partial^2 V_x}{\partial y^2} + \frac{\partial^2 V_x}{\partial z^2} \right) - \frac{1}{Da Re} V_x - \frac{F}{\sqrt{Da}} V_x |\vec{V}| \quad (2)$$

In Y-direction

$$\frac{1}{\varepsilon^2} (V_x \frac{\partial V_y}{\partial x} + V_y \frac{\partial V_y}{\partial y} + V_z \frac{\partial V_y}{\partial z}) = -\frac{\partial p}{\partial y} + \frac{1}{\varepsilon Re} \left( \frac{\partial^2 V_y}{\partial x^2} + \frac{\partial^2 V_y}{\partial y^2} + \frac{\partial^2 V_y}{\partial z^2} \right) - \frac{1}{Da Re} V_y - \frac{F}{\sqrt{Da}} V_y |\vec{V}| \quad (3)$$

In Z-direction

$$\frac{1}{\varepsilon^2} (V_x \frac{\partial V_z}{\partial x} + V_y \frac{\partial V_z}{\partial y} + V_z \frac{\partial V_z}{\partial z}) = -\frac{\partial p}{\partial z} + \frac{1}{\varepsilon Re} \left( \frac{\partial^2 V_z}{\partial x^2} + \frac{\partial^2 V_z}{\partial y^2} + \frac{\partial^2 V_z}{\partial z^2} \right) - \frac{1}{Da Re} V_z - \frac{F}{\sqrt{Da}} V_z |\vec{V}| \quad (4)$$

• Energy equations

Energy equation of the fluid in the porous medium (LTNE) is:

$$(V_x \frac{\partial T_f}{\partial x} + V_y \frac{\partial T_f}{\partial y} + V_z \frac{\partial T_f}{\partial z}) = \frac{(1 + k_f)}{Pr Re} \left( \frac{\partial^2 T_f}{\partial y^2} + \frac{\partial^2 T_f}{\partial z^2} \right) + \frac{h_{sf} a_{sf}}{K_{sf} Pr Re} (T_s - T_f) \quad (5)$$

Energy equation of the solid matrix (LTNE) is:

$$0 = \frac{\partial^2 T_s}{\partial y^2} + \frac{\partial^2 T_s}{\partial z^2} + \frac{h_{sf} a_{sf}}{K_{se}} (T_f - T_s) \quad (6)$$

The equation of energy for an incompressible fluid can be written in the form of a thermal equation for static temperature (without foam):

$$(\mathbf{u} \cdot \nabla) T = \alpha \nabla \cdot (\nabla T) \quad (7)$$

Meshing the Geometry

Using the software SolidWorks2022, the annular model is drawn and then loaded into Ansys Fluent as geometry. To

obtain the optimum convergent solution, a suitable mesh is employed. The model geometry's three-dimensional mesh, as seen in Figure 1, was created using hexahedron and tetrahedron mesh technology. Temperature accuracy is increased by utilizing (inflation and sizing) to control the mesh's form. To test for mesh independence, a smaller size to element was developed. Comparing the average Nusselt numbers of the solutions for various mesh models showed that an element-sized grid with a size of around (1.3mm) was the best mesh. Depending on the cases that were analyzed, the number of pieces ranged from 3,400,000 to 4,700,000.

Validation

Firstly, the work is validated using the inputs and geometry of a smooth double pipe heat exchanger for one of the experimental previous studies presented in Ebieta et al. [23]. The validation process showed a significant accuracy of the simulation model where the error percentage was no more than 2.3%. Validation results are shown in Figure 2.

Setting General

Atmospheric pressure, steady state time, and absolute velocity are taken into account in the four parallel processes and double precision solver that was chosen, the gravitational field (-g) in the (Y) direction. Selecting the energy equation activates the choice of governing models (energy and viscous), the k-realizable model [26] is suitable with the turbulent flow inner the DPHX, and an LTNE model was taken into account. Thus, the velocities coefficients represented by viscous resistance which is the inverse of permeability, inertial resistance, and the interfacial surface area ( $a_{sf}$ ) must be defined by calculate Equations (8-12) and interfacial heat transfer coefficient ( $h_{sf}$ ) was specified from user define file (UDF) as a variable function with velocity as where in (ANSYS FLUENT User's Guide).

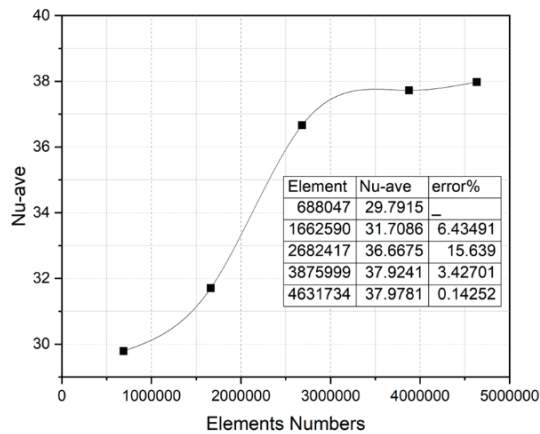
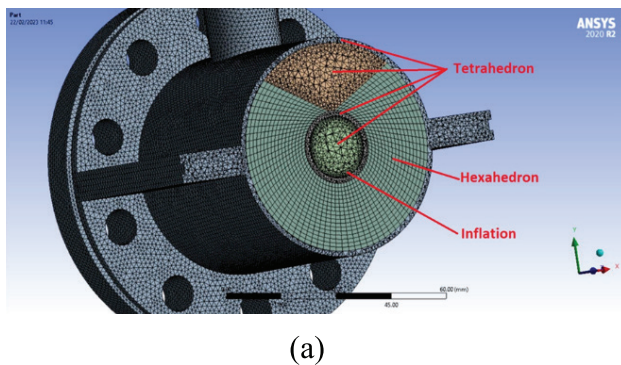


Figure 1. (a) Grid generated for the present model (b) Mesh Dependency.

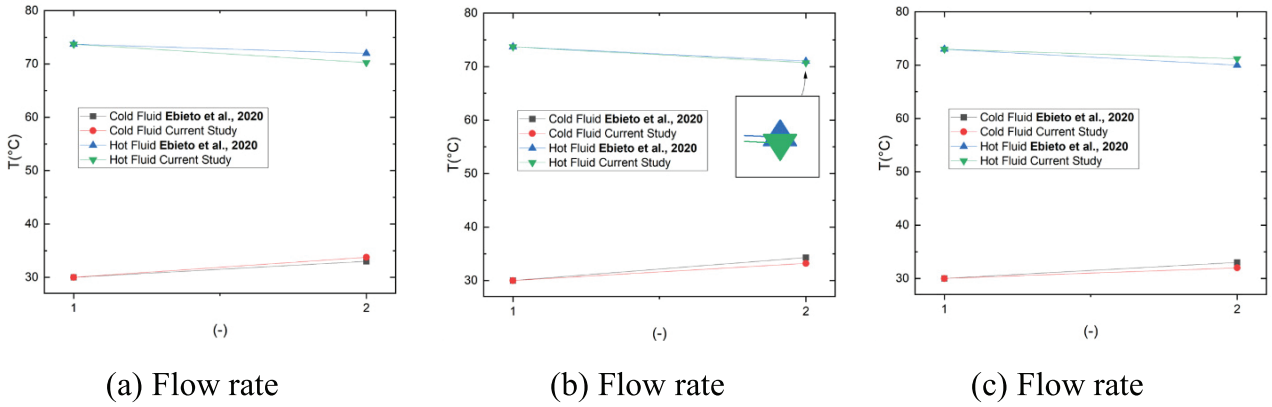


Figure 2. Validation to Ebieto et al. [23].

$$k = 0.00073 dp^2(1 - \varepsilon)^{-0.224} \left[ \frac{d_f}{d_p} \right]^{-1.11} \quad (8)$$

$$F = 0.00212 (1 - \varepsilon)^{-0.132} \left[ \frac{d_f}{d_p} \right]^{-1.36} \quad (9)$$

$$a_{sf} = \frac{3\pi d_f}{(0.59d_p)^2} \left[ 1 - e^{-(1-\varepsilon)/0.04} \right] \quad (10)$$

$$\text{Viscous resistance} = \frac{1}{k} \quad (11)$$

$$\text{Inertial resistance} = \frac{2F}{k^2} \quad (12)$$

**Boundary Conditions**

This section formulates the applicable dimensional boundary conditions at the annule’s inlet, and the outflow, as well as along its walls.

While the outer surface of the inner pipe transfers heat by forced convection, the outer surface of the outer pipe is insulated (q=0). Through conduction, heat passes from the inner surface of the inner pipe to its outer surface and subsequently to the metal foam baffles. The inner pipe’s ends are not taken into consideration. According to White et al. [27], in no-slip conditions, along the inner pipe surface of the inner pipe, the fluid aligned with the walls is stationary, resulting in zero velocity components and the fluid and copper foam temperature is equal to the wall temperature.

Similar to above, the fluid aligned with the walls is stationary along the inner surface of the outer pipe due to the no-slip condition. This means the velocity components are equal to zero. There is no possibility of heat transfer through the outside pipe wall because of the insulation on its outside.

The inlet boundary conditions were (75°C and 30°C) as inlet temperatures to both hot and cold water respectively, and (2 lpm) for the flow rate with insulated outer pipe. The primary variables used to describe the boundary conditions of inlet turbulent flow are provided in Table 2 and Figure 3.

Table 2. Boundary Conditions (B.C.)

Zone	Type	Momentum B.C.	Thermal B.C
cold-inlet	mass-flow-inlet	- Gage Pressure=0 Pa. - Reference: Absolute - Method: Normal to Boundary	Temperature
hot-inlet	mass-flow-inlet	- Gage Pressure=0 Pa. - Reference: Absolute - Method: Normal to Boundary	Temperature
cold-outlet hot-outlet	outflow	-	-
wall-outer-pipe	wall	Stationary, No slip	Insulated No heat flux
wall-inner-pipe	wall	Stationary, No slip	via system coupling

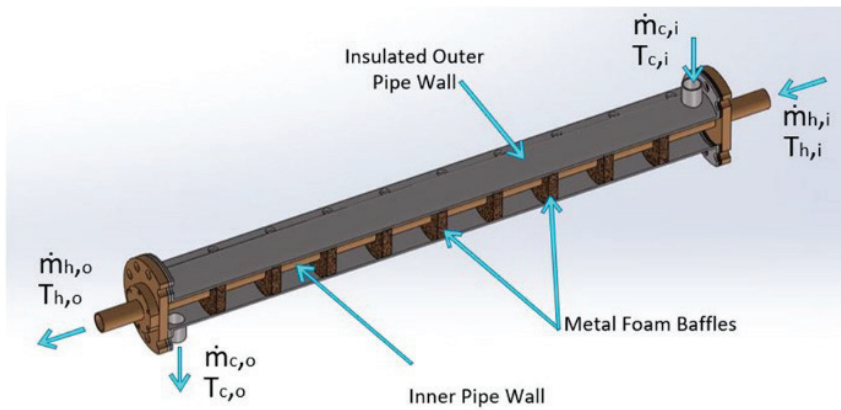


Figure 3. Boundary conditions of geometrical model with metal foam baffles.

**Operating Conditions and Convergence Criterion**

The operating pressure was 101.325 kPa, with a gravity equal to 9.81 in the Y-direction and ambient temperature. The solver tests for convergence of the solution using the residuals technique, utilizing the set of residual values below, and ends when the average residuals drop. The error in the calculation is referred to as “residuals”. If the residuals are less than  $10^{-4}$  and  $10^{-5}$ , it is permitted. The convergence is considered to be  $(10^{-6})$  to the pressure residual and  $(10^{-3})$  to the other residuals, as shown in Figure 4 [26], where the time spent ranged from one to three hours depending on the case.

Four surface temperatures ( $T_{S1}$ ,  $T_{S2}$ ,  $T_{S3}$ , and  $T_{S4}$ ) on the inner pipe. Inlet and outlet water temperature ( $T_{h,i}$ ,  $T_{h,o}$ ,  $T_{c,i}$ , and  $T_{c,o}$ ) for both pipes and inlet and outlet pressure ( $p_{c,i}$  and  $p_{c,o}$ ) for the outer pipe have been limited for each case as Figure 5.

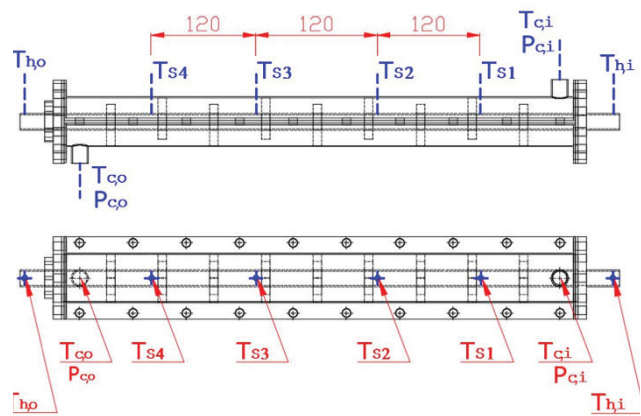


Figure 5. The geometrical model with four surface temperatures.

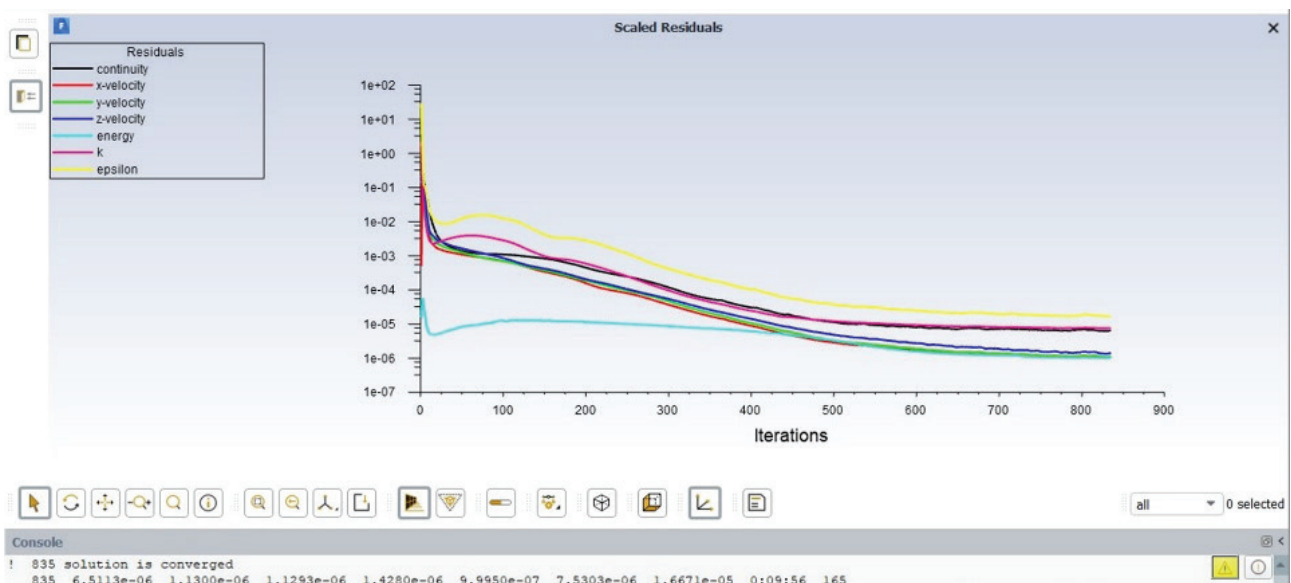


Figure 4. Variation of numerical residuals for different variables with computational iterations.

**Experimental Study**

The experimental setup contains the DPHX test section, heating system, and cooling system. In addition, it contains measurement tools including flow meters, pressure transmitter, and thermometers to measure flow rate, pressure drop, and temperatures respectively, as briefly described in schematically in Figure 6 and graphically in Figure 7.

**The DPHX Test Section**

It consists of (an outer pipe, flanges, an inner pipe, and copper foam baffles) as in 3D drawing Figure 8. The outer pipe was made of stainless steel with an diameter of  $D_o$  (60mm), an inner diameter of  $D_i$  (57mm), and a length of  $L$  (609.6mm), and its outer surface was insulated. Grooves were made inside it with a depth of

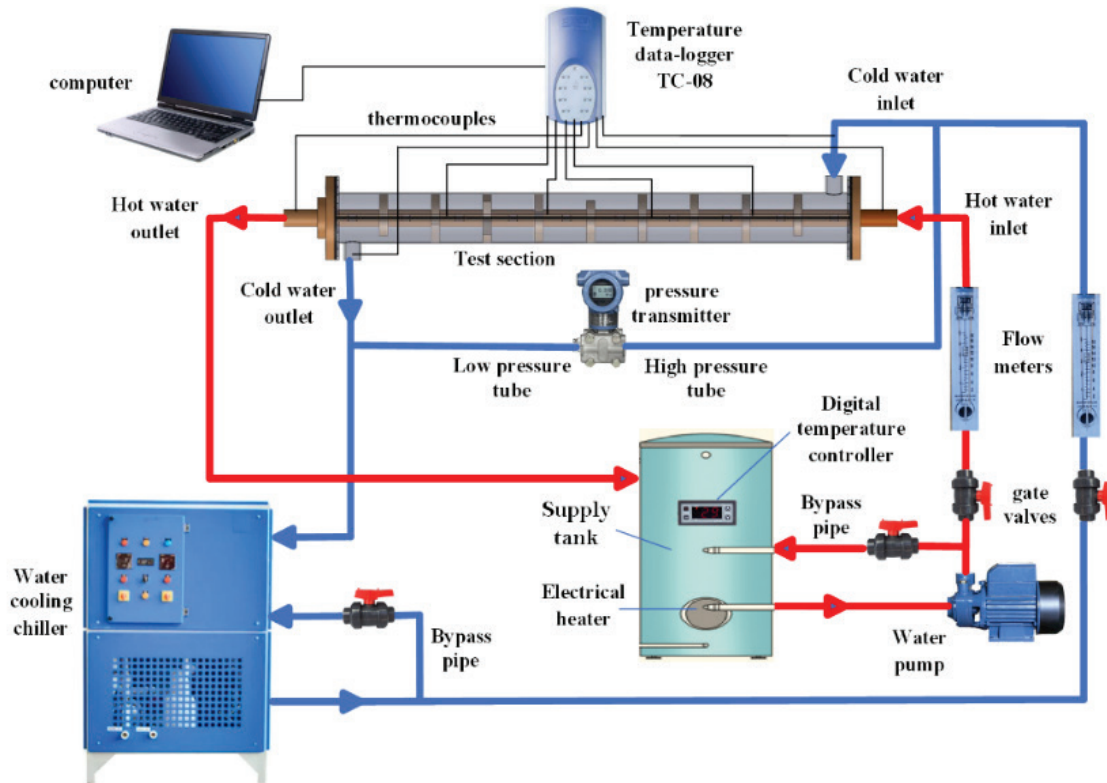
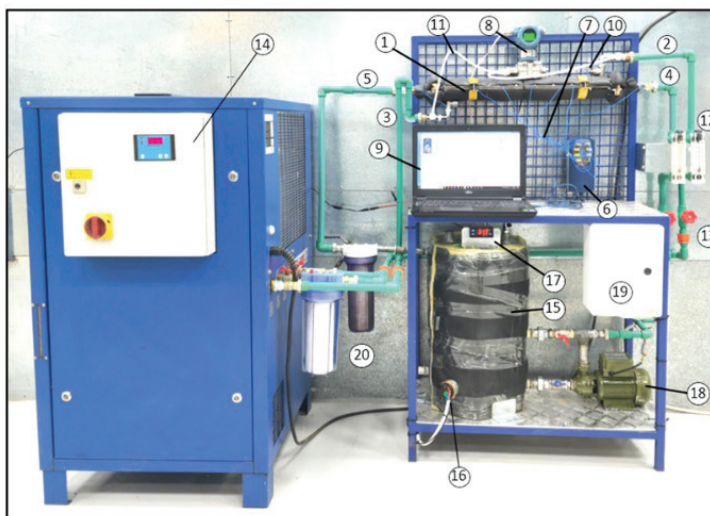


Figure 6. Schematic of experimental apparatus.



1	Test section (DPHX)
2	Cold water inlet
3	Cold water outlet
4	Hot water inlet
5	Hot water outlet
6	Temperature data-logger TC-08
7	thermocouples
8	pressure transmitter
9	computer
10	Low pressure tube
11	High pressure tube
12	Flow meters
13	gate valves
14	Water cooling chiller
15	Supply tank
16	Electrical heater
17	Digital temperature controller
18	Water pump
19	Control panel
20	water filters

Figure 7. Photograph of experimental apparatus.



0.5mm by a lathe machine to fix the CFB in the press-fit bonding method by the external pipe on the CFB [28, 29], and it is cut longitudinally into two halves in symmetry with semi-circular flanges and two rectangle plates on the longitudinal sides was fixed by welding as showed in Figure 9. It is uses bolts and nuts (M8) to connect the two pipe parts with a rubber gasket in between. This method helps in repeating the practical experiment using the same CFB after re-cutting or replacing it. Four holes with a diameter of (2 mm) were made in the upper half with equal dimensions for thermocouple cables then fix the cables by Epoxy adhesives.

The two sides of the outer pipe were closed by flanges made of copper with a thickness of (10 mm) as shown in Figure 10, outer diameter (100 mm), and inner diameter (20 mm), containing ten holes with a diameter (9 mm). One of the flanges was connected to the inner pipe by brazing, and the other would be movable with the inner pipe, where an oil seal was placed between the flange and the inner pipe with a plug of copper to hold the oil seal by the bolts.

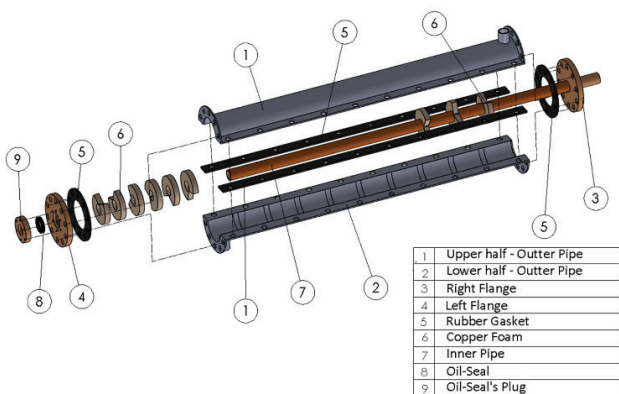


Figure 8. 3D drawing to the DPHX test section.

The copper inner pipe had an outer diameter of  $d_o$  (20 mm), a thickness of (1 mm), and a length of (711mm). Heat-resistant tape with thermal insulation adhesive was used to fix the thermocouple bulbs on it. The CFB are pieces of copper foam as compact discs with inner diameter (19.8 mm), outer diameter (58.2 mm), and thickness (10 mm), and have characteristics (40 PPI, 0.9 porosity), the baffles angles ( $\beta$ ) was made by a cutting machine, all details are shown in Figure 11.

To assemble all parts of the DPHX, one must insert pieces of the CFB their position in with the inner pipe first, then assemble parts of the outer pipe where the CFB is attached with their grooves in the outer pipe. Then, fix the movable flange as shown in Figure 12.

The upstream and downstream ends of the hot water which passes through the inner pipe are connected to the heating system, while those belonging to cold water are connected to the cooling system (Water cooled chiller) through a PVC pipe.

### Heating System

The heating system consists of a supply tank that is made from galvanized iron and of size (38 liters). Glass wool was used as an insulator for the supply tank, (3000W

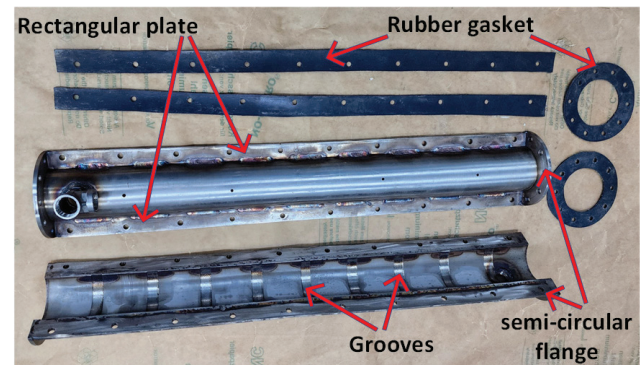


Figure 9. Outer pipe of a DPHX.

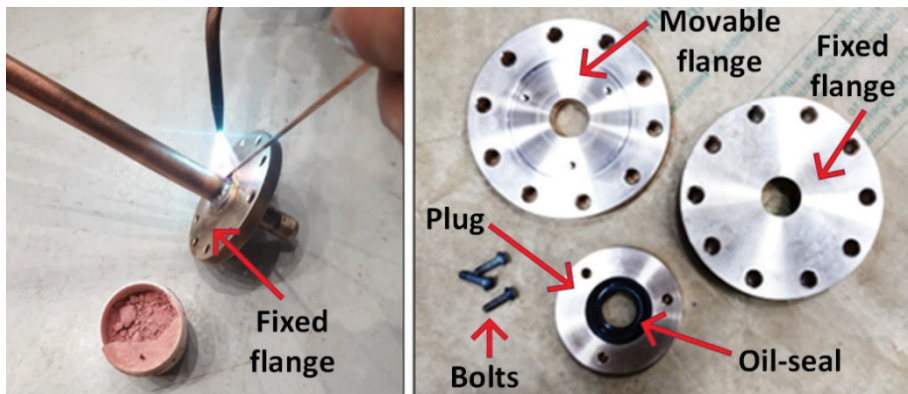


Figure 10. Flanges of a DPHX.

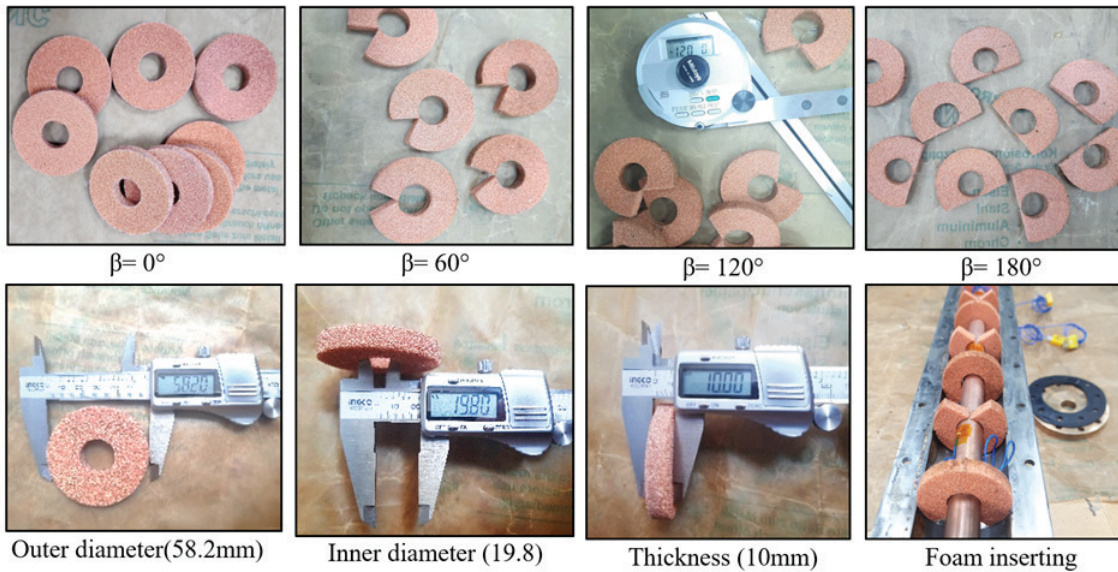


Figure 11. Copper foam baffles.

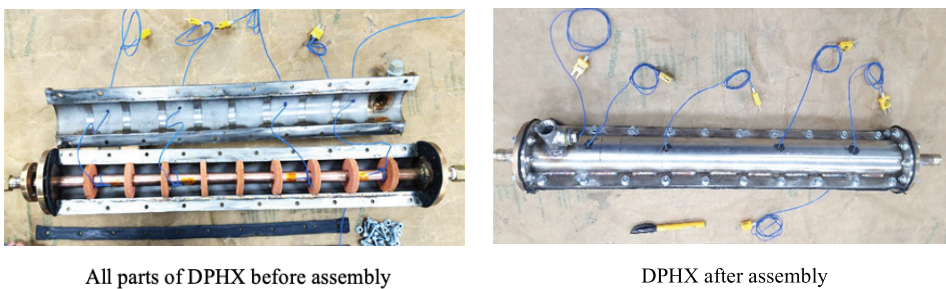


Figure 12. Parts of a DPHX.

AC) electrical heater is used as a heat source, this heater is connected to LCD display digital temperature controller FOX-1004, which has a temperature range (-40°C ~ 90°C) and (220V). the hot water was pumped by (a water pump) with (10-30 l/min) as the flow rate with maximum head (30m). There are two ball valves to control the required exit water flow rate.

**Cooling System**

Water cooled chiller unit (Refrigerant R134a) was used to pump cold water through the outer pipe, it has a pump with pressure (1MPa) with discharge (1.7m3/h), and there are two ball valves to control the flow rate.

**Measuring Devices**

To evaluate the performance of the DPHX with the CFB, many parameters, such as pressure drop, temperature, and flow rate, had to be recorded. A flow meter has a simple structure, no moving parts, no cut-off, and no flow-blocking parts, so there is no pressure loss. It was manufactured from Acrylic material with a flow rate range (2-18 lpm) to

read the differential pressure between the inlet and outlet of cold water. The pressure transmitter has been used with specifications: model (QYb400), rang (-35...35 Kpa), output (4-20mA & Hart), power supply (12-30VDC), Accuracy (0.075% F.S). Temperature measurement and recording with (TC-08 thermocouple data logger) is very easy by using a USB port on a computer to connect and power and using (Picolog program) on Windows software. It has eight channel thermocouples and measures from (-270°C to +1820°C) with high resolution and accuracy. Type k Bare wire thermocouples have been used.

**Experimental Procedure**

At first, the surrounding conditions should be taken into account, particularly the room temperature. It should be close to the cold water temperature, otherwise, more attention should be paid to the heat exchanger’s isolation from the outside environment. The experiment is conducted according to the following steps:

- The water level in the cooling and heating systems should be checked to ensure that they are both at the proper level.
- To prevent any leaks, all of the electrical components and the pipeline must be checked by switching on both systems for some moments.
- Switch on the heating and cooling system to achieve the required temperatures for the hot water and cold water.
- Set the flow rate for both hot water and cold water by adjusting the valve to the required flow rate.
- The system should reach its steady state temperature before taking any readings. This may occur after 35 to 40 minutes at an ambient temperature of 33°C.
- As soon as the system enters a steady state, start recording the temperature results represented by hot water and cold water temperature at inlet and outlet of the DPHX ( $T_{h,i}$ ,  $T_{h,o}$ ,  $T_{c,i}$ , and  $T_{c,o}$ ) and outer surface temperature for inner pipe ( $T_{S1}$ ,  $T_{S2}$ ,  $T_{S3}$ , and  $T_{S4}$ ) and switch on the pressure transmitter to record the pressure results at inlet and outlet cold water ( $p_{c,i}$  and  $p_{c,o}$ ).
- Repeat all the above steps for each experimental case.

### Mathematical Calculations

To complete the mathematical representation of the physical problem some of the partial differential Equations (13-27) must be solved as in below:

### Thermal performance calculation

• The heat transfer rate calculations were according to the following procedure [11, 19]:

Heat transfer of the hot water ( $Q_h$ ) is:

$$Q_h = (\dot{m}C_p)_h (T_{h,i} - T_{h,o}) \quad (13)$$

Heat transfer to cold water ( $Q_c$ ) is:

$$Q_c = (\dot{m}C_p)_c (T_{c,o} - T_{c,i}) \quad (14)$$

• The average heat transfer rate ( $Q_{ave}$ ) is:

$$Q_{ave} = \frac{Q_h + Q_c}{2} \quad (15)$$

• The maximum of heat transfer ( $Q_{max}$ ) is :

$$Q_{max} = (\dot{m}C_p)_h (T_{h,i} - T_{c,i}) \quad (16)$$

• The effectiveness (E) is obtained from :

$$E = \frac{Q_{ave}}{Q_{max}} \quad (17)$$

• The convection heat transfer coefficient ( $h_i$ ) at copper pipe is:

$$h_i = \frac{Q_{ave}}{A_i(T_{h,ave} - T_{s,ave})} \quad (18)$$

• The log mean temperature difference ( $\Delta T_{LM}$ ) for parallel flow is:

$$\Delta T_{LM} = \frac{(T_{h,i} - T_{c,i}) - (T_{h,o} - T_{c,o})}{\ln[(T_{h,i} - T_{c,i}) / (T_{h,o} - T_{c,o})]} \quad (19)$$

• The overall heat transfer coefficient ( $U_i$ ) is:

$$U_i = \frac{Q_{ave}}{A_i \Delta T_{LM}} \quad (20)$$

• The outer convection heat transfer coefficient of cold water ( $h_o$ ) is:

$$h_o = \frac{1}{A_o \left( \frac{1}{U_i A_i} - \frac{1}{h_i A_i} - \frac{\ln\left(\frac{d_o}{d_i}\right)}{2\pi KL} \right)} \quad (21)$$

• The hydraulic diameter ( $D_h$ ):

$$D_h = \frac{4A_c}{p}, A_c = \left(\frac{\pi}{4}\right)(D_i^2 - d_o^2) \quad (22)$$

$$D_h = \frac{4A_c}{p} = \frac{4 \times \left(\frac{\pi}{4}\right)(D_i^2 - d_o^2)}{\pi D_i + \pi d_o} = D_i - d_o \quad (23)$$

• The average Nussle number ( $Nu_{ave}$ ) at the annular pipe is:

$$Nu_{ave} = \frac{h_o D_h}{K_f} \quad (24)$$

### Hydraulic performance calculation

• The velocity ( $u$ ) was estimated using the following equation [11]:

$$u = \frac{\dot{V}}{A_c} = \frac{4\dot{V}}{\pi(D_i^2 - d_o^2)} \quad (25)$$

• The friction factor ( $f$ ) at the annular pipe is:

$$f = \frac{\Delta P \left(\frac{D_h}{L}\right)}{\frac{\rho u^2}{2}} \quad (26)$$

Where  $\Delta P$ : Pressure drop (pa).

### Performance evaluate criteria (PEC) calculation

• The performance evaluate criteria of the double-pipe heat exchanger (PEC) is:



$$PEC = \frac{\left(\frac{Nu_{MF}}{Nu_s}\right)}{\left(\frac{f_{MF}}{f_s}\right)^{\frac{1}{3}}} \quad (27)$$

**Uncertainty analysis**

Every part of the measuring apparatus has an individual accuracy. Holman’s analysis must be applied to account for this accuracy (Holman [30]), as explained in Equations (28-29).

$$R = x_1^{a_1} x_2^{a_2} \dots x_n^{a_n} \quad (28)$$

$$\frac{\omega_R}{R} = \left[ \sum \left( \frac{a_i \omega_{x_i}}{x_i} \right)^2 \right]^{\frac{1}{2}} \quad (29)$$

where

$\frac{\omega_R}{R}$  : is the total error.

$x_i$  : is the error of each independent variable.

$n$  : is the number of total variable.

The results of this investigation indicated that the measurement errors were under 10%. The uncertainty of the devices used in these tests is displayed in Table 3.

**Table 3.** Instrument uncertainties

Independent parameter	Uncertainty
Temperature (T)	± 0.06 °C
Volume flow rate of water inlet	± 0.2 lpm
Pressure drop	± 0.5mpa

**RESULTS AND DISCUSSION**

**Numerical Results**

In this study, three parameters were discussed, including those related to properties of CFB (pore density PPI), and others related to the design of a CFB (baffle angle  $\beta$  and baffle thickness  $t$ ) and the effect of volumetric flow rate ( $\dot{V}$ ) on the thermal performance which included ( $Q_{ave}$ ,  $Nu_{ave}$ , and  $E$ ), hydraulic performance which included ( $\Delta p$  and  $f$ ), and performance evaluate criteria (PEC) to reach an OPHX.

**Thermal performance**

- Effect of baffle angle ( $\beta$ ) at various pore density (PPI)

In Figure 13, the baffle angle was increased by ( $0^\circ$ ,  $60^\circ$ ,  $120^\circ$ , and  $180^\circ$ ) with an increase in pore density by (10, 20, 30, 40, and 50PPI) for each angle. It is proposed that ( $\dot{V} = 2$  lpm and  $t=10$ ). It was observed that heat transfer rate, Nusselt number, and effectiveness increase when the pore density increases and the baffle angle decreases. However, the influence of baffle angle becomes less at pore density between (40 and 50PPI). This can be attributed to the increase in surface area of a CFB when pore density increases and baffle angle decreases.

- Effect of baffle thickness ( $t$ ) at various pore density (PPI)

In Figure 14, baffle thickness was increased as (10, 20, and 30mm) with the same increase in pore density and it is proposed that ( $\dot{V} = 2$  lpm,  $\beta = 180^\circ$ ). For every thickness, it is observed that, as pore density increases, the heat transfer rate, Nusselt number, and effectiveness increase significantly and then become nearly constant and gradually decrease in some cases. This discontinuation in growing up can be attributed to the obstruction of water flow which consequently causes a decrease in these parameters. It is worth mentioning here from the previous results that the shape and volume of a CFB have a significant impact on thermal performance. It can be concluded from the results

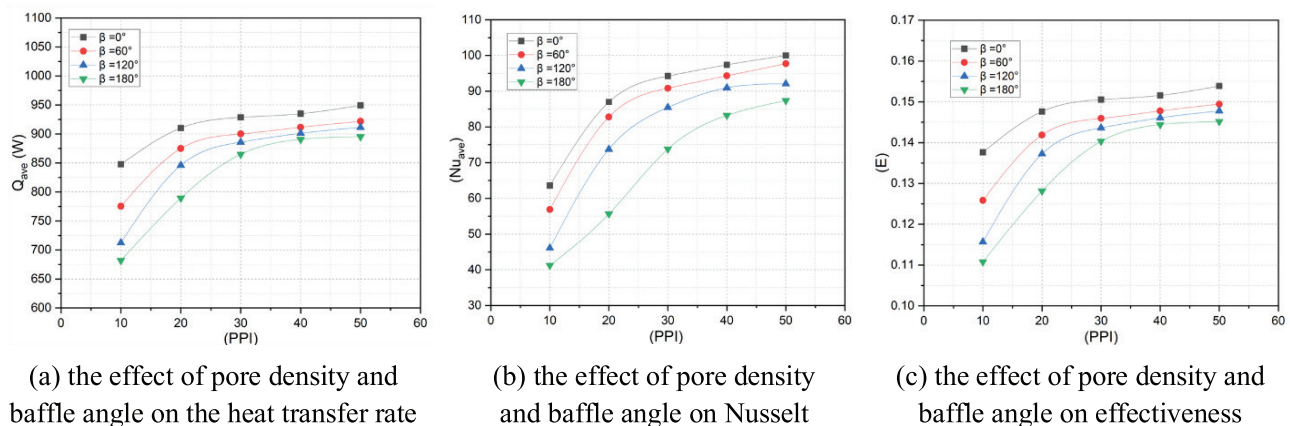


**Figure 13.** The effect of parameters ( $\beta$ , PPI) on the thermal performance.



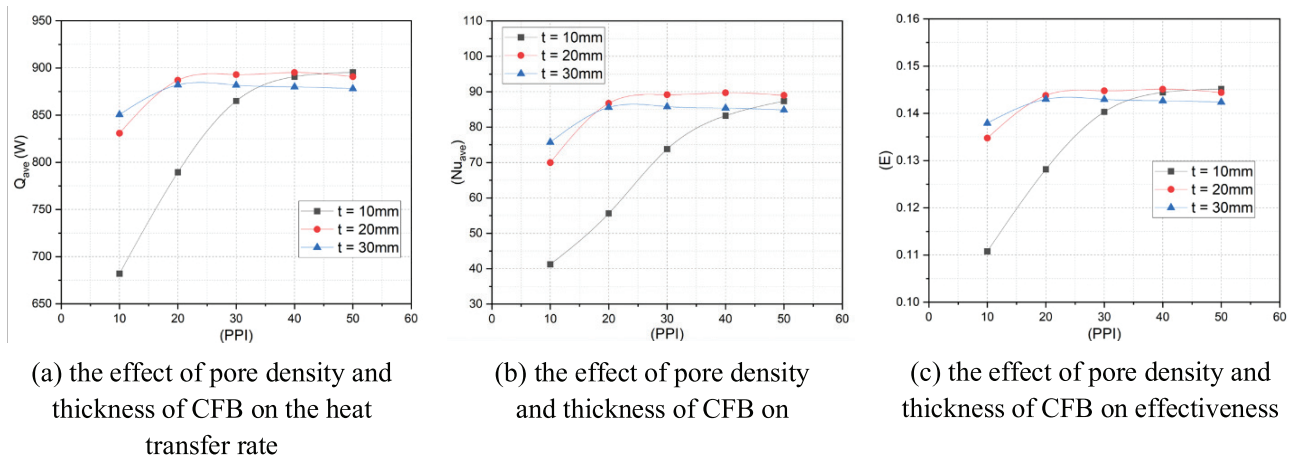


Figure 14. The effect of parameters (t, PPI) on the thermal performance.

that using a CFB with ( $\beta=180^\circ$  and  $t=10\text{mm}$ ) at pore density (50 and 40PPI) resulted in the best thermal performance.

**Hydraulic performance**

A fair comparison has been made between heat transfer rate and Nusselt number improvement versus the rise in the pressure drop as well as the friction factor. It is worth noting that when PEC is less than unity, It represents a negative thermal design for a DPHX with a CFB.

- Effect of baffle angle ( $\beta$ ) at various pore density (PPI)

Figure 15. shows a gradual increase in both the pressure drop and the friction factor as the baffle angle decreases and pore density increases. This is because the friction factor is a function of the pressure drop. The lowest pressure drop and friction factor are seen at ( $\beta=180^\circ$ ). This can be explained as that when porosity density increases, the number of struts surrounding the cell increases also which leads to the increase of friction and curbing of water passage through baffles.

- Effect of thickness of CFB (t) at various pore density (PPI)

In Figure 16, both the pressure drop and friction factor were increased with increased baffles thickness and pore density, and there is a slowdown in the increase after the pore density (30PPI) with the thicknesses (20 and 30mm), but still thickness (10mm) achieved the less the pressure drop and the friction factor.

**Performance evaluate criteria (PEC)**

- Effect of baffle angle ( $\beta$ ) and baffles thickness (t) at various pore density (PPI) and flow rate ( $\dot{V}$ )

Figure 17 shows the PEC of the heat exchanger under the effect of ( $\beta$ , t, and  $\dot{V}$ ). Figure 17a and Figure 17b shows that the performance evaluate criteria have reached their maximum value (PEC=1.88) at (40PPI,  $\beta=180^\circ$ ,  $t=10\text{mm}$ ) despite the opposed effect of high pressure drop, and this is considered the optimal engineering design in this current study. In Figure 17c, the effect of the flow rate ( $\dot{V}=2\text{-}6\text{ lpm}$ ) has been illustrated and the highest (PEC=2.16) was found

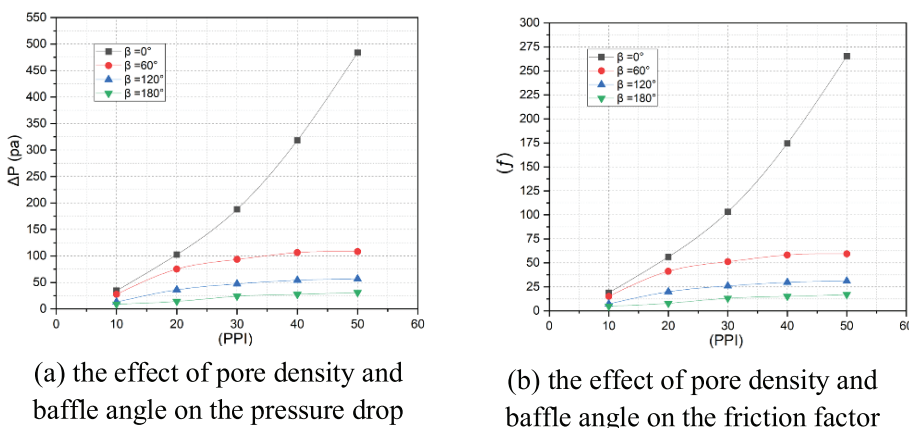


Figure 15. The effect of parameters ( $\beta$ , PPI) on hydraulic

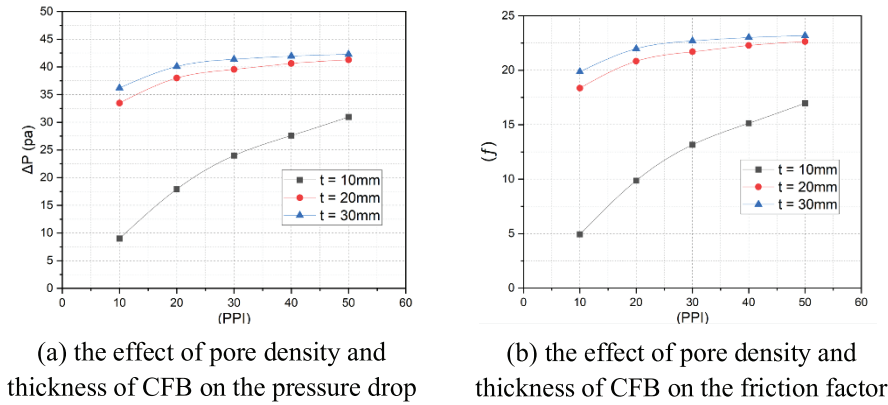


Figure 16. The effect of parameters ( $\beta$ , PPI) on hydraulic performance.

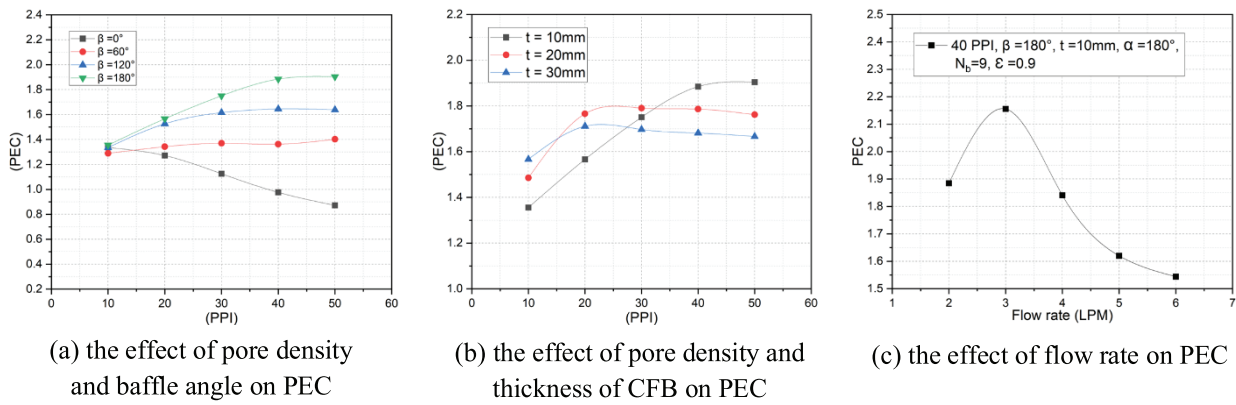


Figure 17. The effect of parameters ( $\beta$ ,  $t$ , PPI,  $\dot{V}$ ) on performance evaluate criteria (PEC).

at a flow rate (3 lpm), After that it is noted the decrease in PEC was when the volumetric flow rate increases more than (3 lpm).

## COMPARISON RESULTS

### Thermal A comparison of thermal performance and hydraulic performance in the three heat exchangers

The thermal performance, hydraulic performance, and PEC are compared for three kinds of heat exchangers namely, (without foam (HXWOF), with full foam (HXWFF), and optimum design (OPHX)). The compared results are obtained at (40PPI and  $\epsilon=0.9$ ) and flow rate ( $\dot{V}=2-6$  lpm). Figure 18a noted that the average difference in heat transfer rate between a HXWFF and a HXWOF is greater than the difference between an OPHX and a HXWOF by (63%). This behavior was noted in Figure 18b and Figure 18c, where Nusselt number and the effectiveness were (241.5%, and 64.6%) respectively. The penalty for increasing both pressure drop and friction factor was very large in a HXWFF as shown in Figure 18d and Figure

16e, so the judgment of the performance evaluate criterion was in Figure 18f, which gave the largest average PEC to an OPHX which was (72.7%) great than a HXWFF.

### Comparison between experimental results and numerical results

In Figure 19, experimental results and numerical results were compared at ( $\beta=0^\circ, 60^\circ, 120^\circ, 180^\circ$ ), (40PPI,  $\epsilon=0.9$ ), and at a flow rate (2 lpm). It was observed that the average difference between experimental results and numerical results is (11.5%) for thermal performance, (3.5%) for hydraulic performance, and (9.8%) for performance evaluate criteria. The reason for this average difference can be attributed to the using of temperature sensors in the waterway and the use of a press-fit bonding method in contacting the baffles with the outer pipe which might consequently lead to such errors, In addition, such difference can also be attributed to the heat loss to the surrounding during the experimental work. Furthermore, the theoretical assumptions that were taken during simulation can result in such deviation between the experimental and simulation results.

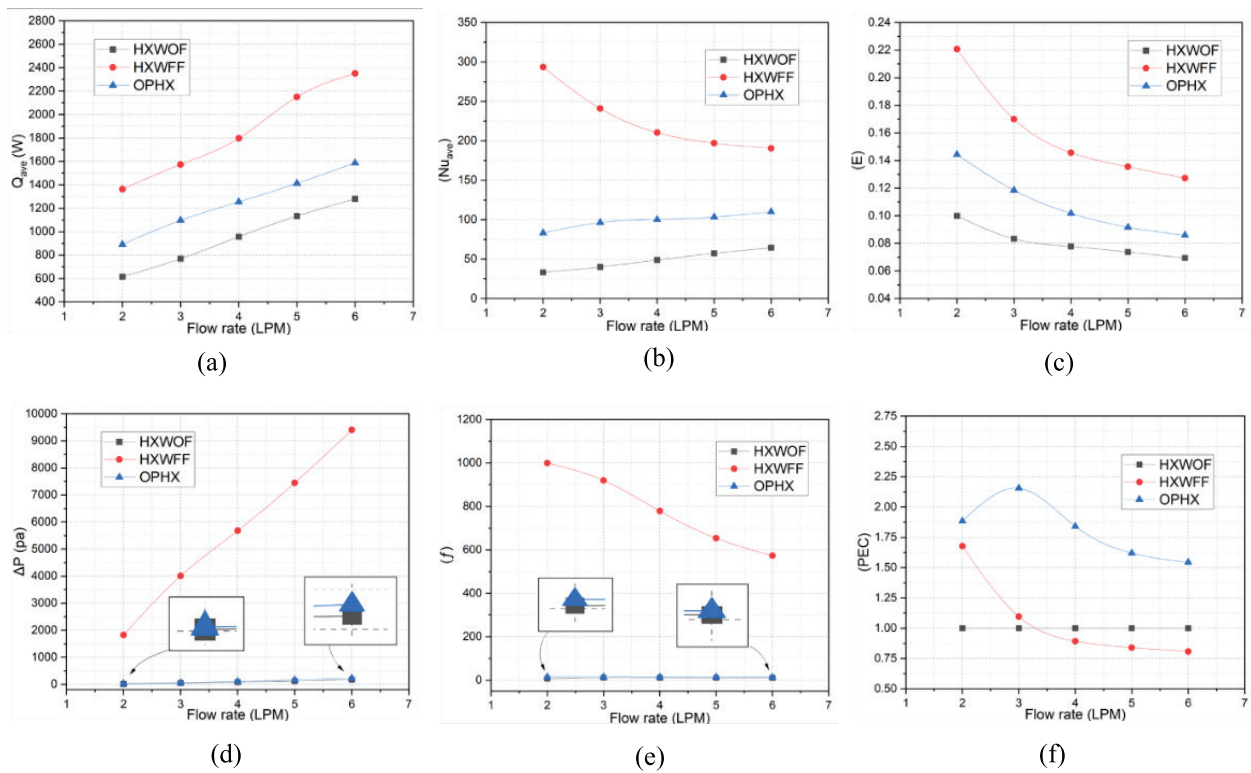


Figure 18. The effect of parameter flow rate ( $\dot{V}$ ) on ( $Q$ ,  $Nu$ ,  $\Delta p$ ,  $f$ , and  $PEC$ ) for a three DPHX.

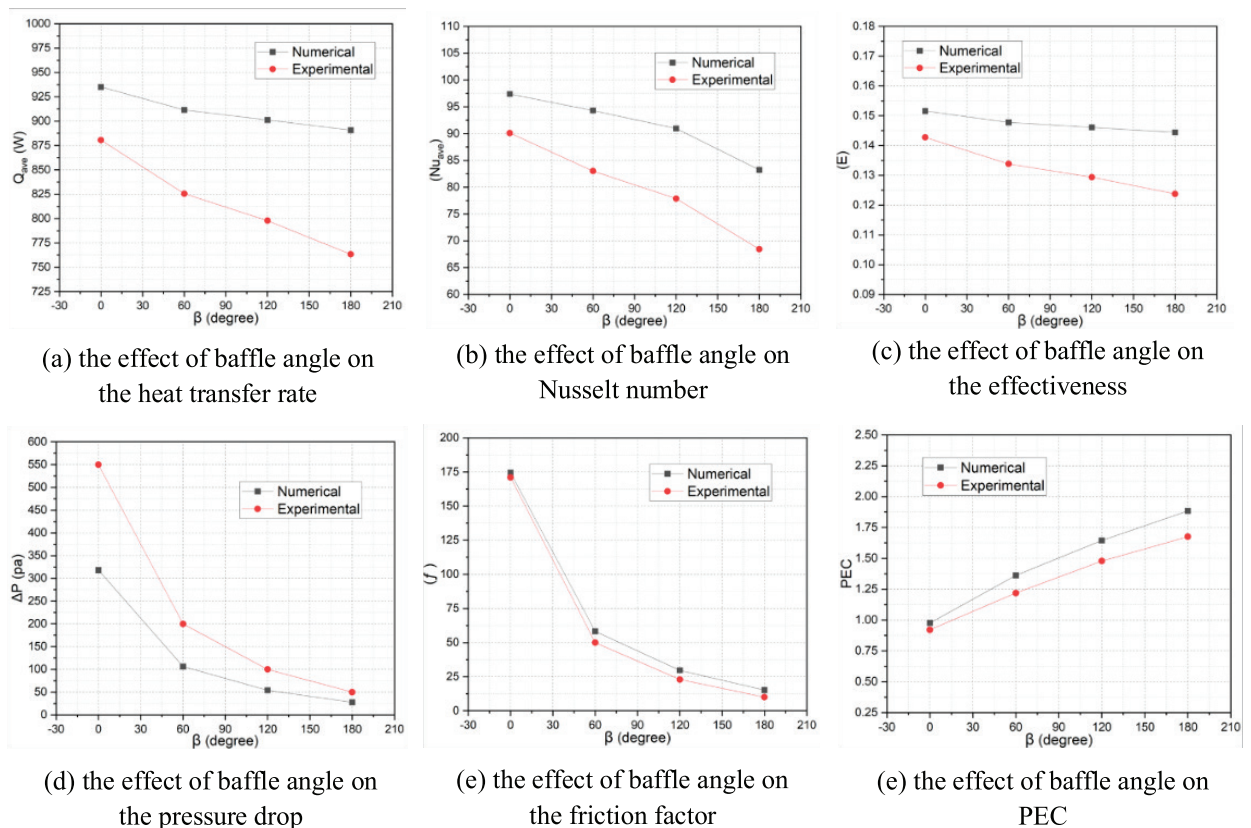


Figure 19. The experimental and numerical results comparison of the effect of baffle angle ( $\beta$ ).



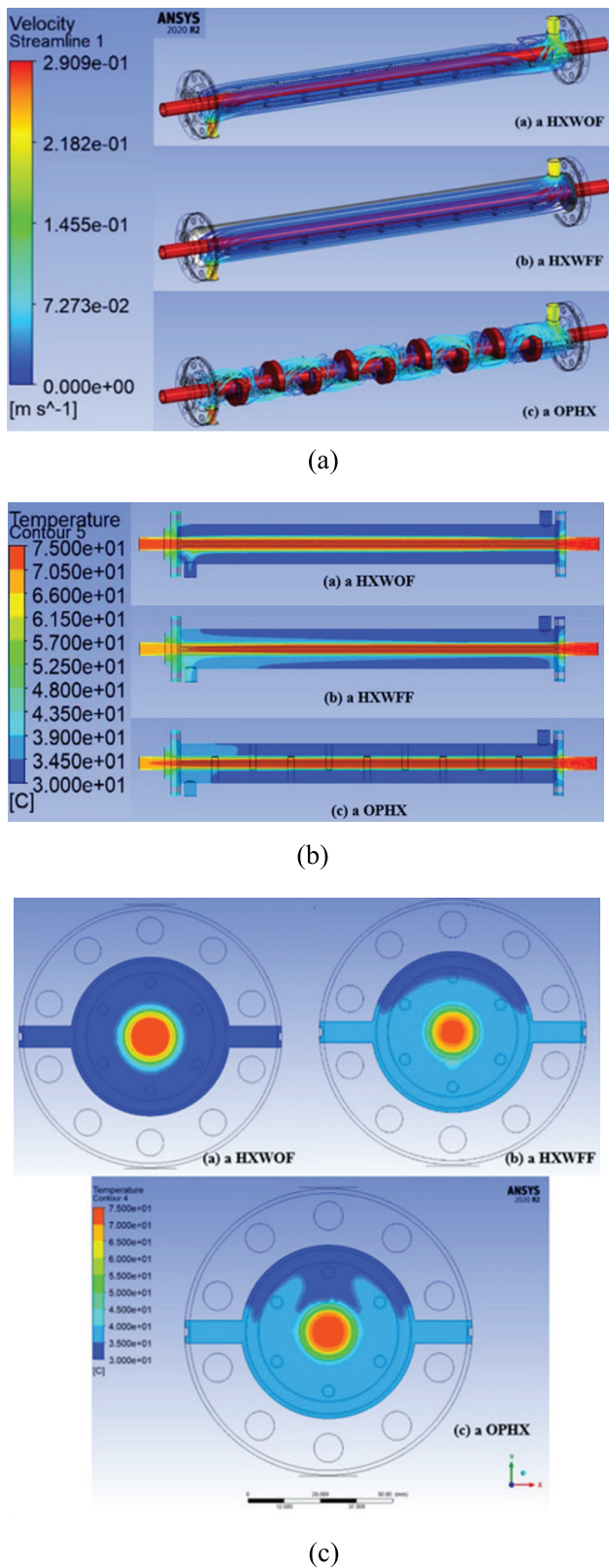


Figure 20. Comparison of fluid velocity streamlines and temperature contour shapes.

This difference generally increases when the baffle angle increases, it can be attributed to the press-fit bonding method [28], where increasing the baffle angles will lead to the weakness of contact between the baffle and the inner surface of the outer pipe. This weakness is due to the reduction of contacting pressure and will cause a reduction in the heat transfer rate. In real-world applications, it is recommended to use the brazing method for permanent fixation as in De Jaeger et al. [28].

**Comparison of velocity streamlines and temperature contours**

The velocity streamlines and temperature contour shapes of the three heat exchangers (HXWOF, HXWFF, and OPHX) are compared for the same properties of copper foam (40PPI and  $\epsilon=0.9$ ) with a flow rate (2 lpm). In Figure 20a, the streamline for (HXWOF and HXWFF), the flow was straight lines shape without vortices and mixing. The decrease of boundary layers can appear. Whereas in an OPHX, the flow was in a sine wave shape which decreases the volume of boundary layers. In Figure 20b, the temperature contour of the three heat exchangers has been illustrated. It was observed that the bluish color was in the largest area in a HXWOF, while this area decreased in an OPHX, and the area was the smallest in the HXWFF. This can be clarified, as the largest heat transfer convection occurs in a HXWFF. In the last Figure 20c, it shows the temperature contour at a plane (X=575 mm pre the fluid exit). The reddish color of the hot fluid was gradual in the inner pipe, where the largest gradient was in a HXWFF.

**CONCLUSION**

A numerical and experimental study of thermal performance assessment of heat exchanger with metal foam has been carried out. The numerical model was validated in comparison with a previously published paper. Then the numerical model was used for conducting a wide investigation on the influence of pore density, baffle angle, and water flow rate on the thermal and hydraulic performance of the double pipe heat exchanger with copper foam. Based on the results obtained in this work, the following conclusions are made:

- Partial filling of annular pipe improves convection heat transfer, reduces the friction factor, and provides better performance evaluate criteria than completely filling. This is due to the heat transfer mechanism through copper foam baffles with their special design and special characteristics that cause fluid mixing and distortion as well as circulation through the annular gap which increases water temperature and no significant penalty of the pressure drop.
- Compared to the completely filled heat exchanger, the thermal and hydraulic performance of the heat exchanger with partial filling of annular pipe is better in terms of higher convection heat transfer rate, lower



friction factor, and better performance evaluate criteria. The reason behind this better performance of heat exchanger with partially filled foam is the heat transfer mechanism through copper foam baffles with their special design and special characteristics. This causes fluid mixing and distortion as well as circulation through the annular gap which consequently increases water temperature and no significant penalty of the pressure drop.

- The average heat transfer rate and Nusselt numbers increase with the increase in pore density, and this also causes an increase in the pressure drop.
- The increase in the volume of copper foam baffles due to an increase in baffle angle and baffle thickness causes an increase in the heat transfer rate and the pressure drop.
- Using these parameters (baffle angle  $\beta=180^\circ$ , thickness of CFB  $t=10\text{mm}$ , Pore density 40PPI, and 3 lpm flow rate) with the optimal heat exchanger (OPHX), the optimum average heat transfer rate, average heat transfer coefficient, Nusselt number, the effectiveness, and performance evaluate criteria were 1096W, 1698.4W/m<sup>2</sup>.°C, 96.4, 0.12, and 2.16 respectively.
- The best of the performance evaluate criteria (PEC) of the optimal heat exchanger (OPHX) was at the flow rate ( $\dot{V} = 3$  lpm) and this the performance evaluate criteria (PEC) decreases when the flow rate is increased or decreased. This behavior did not occur with the heat exchanger with full copper foam (HXWFF), where the performance evaluate criteria (PEC) was decreased as the flow rate increased. This explains the reason for the change in the design of baffles to reach the best condition by reaching the largest flow rate.
- Effect of the average heat transfer rate and Nusselt numbers respectively in the heat exchanger with full foam (HXWFF) was (63% and 241%) which is greater than the optimal heat exchanger (OPHX), while the average performance evaluate criteria in the optimal heat exchanger (OPHX) was (73%) which is greater than the heat exchanger with full foam (HXWFF) due to the high pressure drop at a flow rate (2-6 lpm).
- Experimentally, the percentage of improvement in the heat transfer rate and Nusselt number in the optimal heat exchanger (OPHX) was (33.8% and 96.7%), in comparison the numerically calculated it was (42.6% and 103,8%) at a flow rate (3 lpm). The reason for this average difference is due to the use of temperature sensors and the use of a press-fit bonding method [28]. it is recommended to use the brazing method.

## NOMENCLATURE

$a_{sf}$	Interfacial surface area (1/m)
$A_c$	Cross section area of annular gap (m <sup>2</sup> )
$A_p, A_o$	Inner and outer Surface area of inner pipe (m <sup>2</sup> )
$D_a$	Darcy Number
$D_p, D_o$	Inner and outer diameter of outer pipe (m)

$d_p, d_o$	Inner and outer diameter of inner pipe (m)
$d_f$	Fiber diameter (mm)
$d_p$	Pore diameter (mm)
$F$	Inertial coefficient of metal foam
$f$	Friction factor with metal foam
$f_{MF}$	Friction factor with metal foam
$f_s$	Friction factor without metal foam (smooth)
$h_{sf}$	Interfacial heat transfer coefficient (W/m <sup>2</sup> .k)
$K$	Thermal conductivity (W/m.k)
$k$	Permeability of metal foam (m <sup>2</sup> )
$k_e$	Effective thermal conductivity in metal foam (W/m.k)
$k_{fe}$	Effective thermal conductivity of fluid (W/m.k)
$k_{se}$	Effective thermal conductivity of solid (W/m.k)
$Nu$	Nusselt number
$Nu_{MF}$	Nusselt number with metal foam
$Nu_s$	Nusselt number without metal foam (smooth)
$P_r$	Pyrantel Number
$P_r$	Pyrantel Number
$P_{c,i}, P_{c,o}$	Inlet and Outlet pressure for the outer pipe (pa)
$Q$	Heat transfer rate (W)
$Re$	Renault Number
$t$	Baffles thickness (mm)
$T$	Temperature (°C)
$T_f, T_s$	Temperature of fluid and the solid matrix (K)
$T_{s1}, T_{s2}$	Surface temperature on the inner pipe (°C)
$T_{c,i}, T_{c,o}$	Inlet and outlet cold water temperature (°C)
$T_{h,i}, T_{h,o}$	Inlet and outlet hot water temperature (°C)

## Greek symbols

$\beta$	Baffles angles (degree)
$\rho$	Density (kg/m <sup>3</sup> )
$\mu$	Viscosity (N.S/m <sup>2</sup> )
$\Delta p$	Pressure drop across the heat exchanger (Pa)
$\epsilon$	Porosity of metal foam
$p$	Wetted perimeter (m)
$\dot{V}$	Volumetric flow rate (lpm)

## Subscripts

$i, o$	Inlet and Outlet
$h, c$	Hot and Cold
$ave$	Average
$s$	Surface

## Abbreviations

CFB	Coper foam baffles
DPHX	Double pipe heat exchanger
E	Effectiveness
HXWFF	Heat exchanger with full foam
HXWOF	Heat exchanger without foam
LTNE	Local thermal non-equilibrium
OPHX	Optimal heat exchanger
PPI	pore density
PEC	The performance evaluate criteria
UDF	User define file

## AUTHORSHIP CONTRIBUTIONS

Authors equally contributed to this work.

## DATA AVAILABILITY STATEMENT

The authors confirm that the data that supports the findings of this study are available within the article. Raw data that support the finding of this study are available from the corresponding author, upon reasonable request.

## CONFLICT OF INTEREST

The authors declared no potential conflicts of interest with respect to the research, authorship, and/or publication of this article.

## ETHICS

There are no ethical issues with the publication of this manuscript.

## REFERENCES

- [1] Lande RD, Tamkhade PK, Lele MM. Heat transfer and pressure drop analysis of double tube heat exchanger with and without metal foam in annular space. *Emerging Trends Mech Ind Eng* 2023;361–377. [\[CrossRef\]](#)
- [2] Hassan AM, Alwan AA, Hamzah HK. Numerical study of fan coil heat exchanger with copper-foam. *Int J Fluid Mach Syst* 2023;16:73–88. [\[CrossRef\]](#)
- [3] Chatzi P, Antoniadou A, Efstathiadis T, Kalfas AI. Thermal performance investigation of metal foam heat exchanger for micro-gas turbine. *J Phys Conf Ser* 2023;2511:012013. [\[CrossRef\]](#)
- [4] Mirshekar A, Goodarzi MR, Mohebbi-Kalhari D, Shafiei Mayam MH. Experimental study of heat transfer enhancement using metal foam partially filled with phase change material in a heat sink. *J Energy Storage* 2023;60:106496. [\[CrossRef\]](#)
- [5] Bousri A, Hamadouche A, Khali S, Nebbali R, Beji MH. Forced convection cooling of multiple heat sources using open cell metal foams. *J Therm Eng* 2021;7:255–270. [\[CrossRef\]](#)
- [6] Banerjee A, Diplina P. Heat transfer analysis using a duct filled with metal foams. *J Therm Eng* 2021;8:529–537. [\[CrossRef\]](#)
- [7] Chumpia A, Hooman K. Performance evaluation of single tubular aluminium foam heat exchangers. *Appl Therm Eng* 2014;66:266–273. [\[CrossRef\]](#)
- [8] Arbak A, Dukhan N, Bağcı Ö, Özdemir M. Influence of pore density on thermal development in open-cell metal foam. *Exp Therm Fluid Sci* 2017;86:180–188. [\[CrossRef\]](#)
- [9] Ali RMK, Ghashim SL. Thermal performance analysis of heat transfer in pipe by using metal foam. *JJMIE* 2023;17:205–218. [\[CrossRef\]](#)
- [10] Alibeigi M, Farahani SD. Effect of porous medium positioning on heat transfer of micro-channel with jet. *Int J Eng* 2020;33:2057–2064. [\[CrossRef\]](#)
- [11] Hamzah JA, Nima MA. Experimental study of heat transfer enhancement in double-pipe heat exchanger integrated with metal foam fins. *Arab J Sci Eng* 2020;45:5153–5167. [\[CrossRef\]](#)
- [12] Arasteh H, Salimpour MR, Tavakoli MR. Optimal distribution of metal foam inserts in a double-pipe heat exchanger. *Int J Numer Methods Heat Fluid Flow* 2019;29:1322–3142. [\[CrossRef\]](#)
- [13] Maid IW, Hilal KH, Lafta NS. Numerical analysis for enhancing transferred heat in porous counter flow heat exchanger. *IOP Conf Ser Mater Sci Eng* 2020;745:012081. [\[CrossRef\]](#)
- [14] Chen X, Xia X, Sun C, Wang F, Liu R. Performance evaluation of a double-pipe heat exchanger with uniform and graded metal foams. *Heat Mass Transf* 2020;56:291–302. [\[CrossRef\]](#)
- [15] Farhan TH, Fadhil OT, Ahmed HE. Performance of a double-pipe heat exchanger with different metal foam arrangements. *Anbar J Eng Sci* 2021;9:100–112. [\[CrossRef\]](#)
- [16] Alhusseny A, Turan A, Nasser A. Rotating metal foam structures for performance enhancement of double-pipe heat exchangers. *Int J Heat Mass Transf* 2017;105:124–139. [\[CrossRef\]](#)
- [17] Abandani MHS, Ganji DD. Melting effect in triplex-tube thermal energy storage system using multiple PCMs-porous metal foam combination. *J Energy Storage* 2021;43:103154. [\[CrossRef\]](#)
- [18] Mohammadi MH, Abbasi HR, Yavarinasab A, Pourrahmani H. Thermal optimization of shell and tube heat exchanger using porous baffles. *Appl Therm Eng* 2020;170:115005. [\[CrossRef\]](#)
- [19] Naqvi SMA, Wang Q. Performance enhancement of shell-tube heat exchanger by clamping anti-vibration baffles with porous media involvement. *Heat Transf Eng* 2021;42:1523–1538. [\[CrossRef\]](#)
- [20] Tamkhade PK, Lande RD, Gurav RB, Lele MM. Investigations on tube in tube metal foam heat exchanger. *Mater Today Proc* 2023;72:951–957. [\[CrossRef\]](#)
- [21] Fiedler T, Moore R, Movahedi N. Manufacturing and characterization of tube-filled ZA27 metal foam heat exchangers. *Metals* 2021;11:1277. [\[CrossRef\]](#)
- [22] Zhou F, Lu T, Zhuang D, Ding G. Experimental study of condensation heat transfer characteristics on metal foam wrapped tubes under sloshing conditions. *Int J Heat Mass Transf* 2021;176:121394. [\[CrossRef\]](#)
- [23] Ebieto CE, Ana RR, Nyong OE, Saturday EG. Design and construction of a double pipe heat exchanger for laboratory application. *Eur J Eng Technol Res* 2020;5:1301–1306. [\[CrossRef\]](#)
- [24] Niameh A, Alhusseny M. Heat transfer enhancement using rotating porous media. *University of Manchester*; 2016.p. 233.

- 
- [25] Uglah AM, Jubear AJ. Numerical thermal performance of free convection in metal foam heat sinks with fin edges. *Univ Thi-Qar J Eng Sci* 2020;11:19–30. [\[CrossRef\]](#)
- [26] Ozden E, Tari I. Shell side CFD analysis of a small shell-and-tube heat exchanger. *Energy Convers Manag* 2010;51:1004–1014. [\[CrossRef\]](#)
- [27] White FM, Majdalani J. *Viscous Fluid Flow*. 3rd ed. New York: McGraw-Hill; 2006.
- [28] De Jaeger P, T'Joelens C, Huisseune H, Ameel B, De Schampheleire S, De Paepe M. Assessing the influence of four bonding methods on the thermal contact resistance of open-cell aluminum foam. *Int J Heat Mass Transf* 2012;55:6200–6210. [\[CrossRef\]](#)
- [29] Ahmed HE, Fadhil OT, Farhan TH. Performance of a double-pipe heat exchanger with different metal foam arrangements. *Anbar J Eng Sci* 2021;12:171162. [\[CrossRef\]](#)
- [30] Holman JP. *Experimental Methods For Engineers*. 8th ed. New York: McGraw-Hill; 2011.